Histochemistry and Cell Biology
https://doi.org/10.1007/s00418-018-1686-5

ORIGINAL PAPER

A heart for fibrillin: spatial arrangement in adult wild-type murine myocardial tissue

Felke Steijns[1] · Jolanda van Hengel[2] · Patrick Sips[1] · Julie De Backer[1,3] · Marjolijn Renard[1]

Accepted: 5 June 2018

Abstract

Fibrillins are major constituents of microfibrils, which are essential components of the extracellular matrix of connective tissues where they contribute to the tissue homeostasis. Although it is known that microfibrils are abundantly expressed in the left ventricle of the heart, limited data are available about the presence of microfibrils in the other parts of the myocardial tissue and whether there are age or sex-related differences in the spatial arrangement of the microfibrils. This basic knowledge is essential to better understand the impact of fibrillin-1 pathogenic variants on the myocardial tissue as seen in Marfan related cardiomyopathy. We performed histological analyses on wild-type male and female murine myocardial tissue collected at different time-points (1, 3 and 6 months). Fibrillin-1 and -2 immunofluorescence stainings were performed on cross-sections at the level of the apex, the mid-ventricles and the atria. In addition, other myocardial matrix components such as collagen and elastin were also investigated. Fibrillin-1 presented as long fibres in the apex, mid-ventricles and atria. The spatial arrangement differed between the investigated regions, but not between age groups or sexes. Collagen had a similar broad spatial arrangement to that of fibrillin-1, whereas elastic fibres were primarily present in the atria and the vessels. In contrast to fibrillin-1, limited amounts of fibrillin-2 were observed. Fibrillin-rich fibres contribute to the architecture of the myocardial tissue in a region-dependent manner in wild-type murine hearts. This knowledge is helpful for future experimental set-ups of studies evaluating the impact of fibrillin-1 pathogenic variants on the myocardial tissue.

Keywords Microfibrils · Fibrillin-1 · Cardiac tissue · Spatial arrangement · Myocardial ECM

Introduction

The myocardial extracellular matrix (ECM) represents a complex three-dimensional network of various macromolecules in close interaction with each other and neighbouring cardiac myocytes. The myocardial ECM can be subdivided into two areas: the perimysium and the endomysium (Purslow 2008). The perimysium is a layer of connective tissue associated with bundles of cardiac myocytes thereby providing a laminar architecture of muscle layers. The endomysium surrounds and interconnects individual cardiac myocytes to neighbouring cells and capillaries. This close interaction between the myocardial ECM and the cardiac myocytes allows transmission of a plethora of signals from the extracellular environment to the cardiac myocyte, thereby influencing the cellular morphology and function (Borg et al. 1996). In addition, in response to local cell signals the myocardial ECM also changes continuously, creating a dynamic responsive entity (Pope et al. 2008). Coordinated interplay between the signals originating from both the myocardial ECM and the cardiac myocytes is crucial for a normal cardiac function (Pope et al. 2008).

An important component of the myocardial ECM is the protein fibrillin-1 (Bouzeghrane et al. 2005; Vracko et al. 1990; Lockhart et al. 2011). Previously, Bouzeghrane et al. demonstrated by means of immunohistochemistry that fibrillin-1 is abundantly present in the ventricular myocardium of

Electronic supplementary material The online version of this article (https://doi.org/10.1007/s00418-018-1686-5) contains supplementary material, which is available to authorized users.

✉ Felke Steijns
Felke.steijns@Ugent.be

[1] Center for Medical Genetics, Ghent University Hospital, Ghent, Belgium

[2] Department of Basic Medical Sciences, Faculty of Medicine and Health Sciences, Ghent University, Ghent, Belgium

[3] Department of Cardiology, Ghent University Hospital, Ghent, Belgium

Published online: 20 June 2018

male wild-type adult rats. Furthermore, they reported a significant increase in fibrillin-1 synthesis in male rats with cardiac fibrosis and suggested that fibrillin-1 serves an important role in cardiac tissue repair (Bouzeghrane et al. 2005). Vracko et al. localized high amounts of fibrillin-1, also by means of immunohistochemistry, at the level of the papillary muscle of both female and male adult patients obtained after transplantation for ischemic heart disease. As the papillary muscle contains many anchorage points between the cardiac myocytes and the collagen fibres of the chordae tendineae, the abundance of fibrillin-1 in this specific area, therefore, suggests that fibrillin-1 serves an important role in transmitting forces from the ECM to cardiac myocytes (Vracko et al. 1990).

In humans, three fibrillin genes (*FBN1, -2* and *-3*) encoding fibrillin-1, -2 and -3, respectively, have been identified (Cain et al. 2006; Sakai et al. 2016). Fibrillin-1 is expressed from gastrulation throughout postnatal life (Sakai et al. 2016; Cain et al. 2006; Ramirez and Pereira 1999). Whereas, fibrillin-2 is mainly expressed during foetal development with only limited expression in postnatal tissues (Zhang et al. 1994). Fibrillin-3 is exclusively expressed in foetal tissue (Sakai et al. 2016; Cain et al. 2006). In mice, there are only two *Fbn* genes, *Fbn1* and *Fbn2*. The *Fbn3* gene has been inactivated in the mouse genome during evolution (Corson et al. 2004).

Fibrillins are the principal components of the 10–12 nm diameter extracellular matrix microfibrils (Cain et al. 2006; Hubmacher et al. 2008; Sakai et al. 1986, 2016; Sherratt et al. 2001). Microfibrils are highly conserved macromolecules distributed in all dynamic connective tissues, either associated with elastin in elastic fibres or as elastin-free microfibrils in non-elastic tissues subjected to repeated mechanical stress (Jensen and Handford 2016; Sherratt et al. 2001; Ramirez and Pereira 1999).

To date, although fibrillin-1 dysfunction has been linked to myocardial disease, the exact spatial arrangement of fibrillin-1 in the myocardial tissue remains largely unknown (Campens et al. 2015; De Backer et al. 2006). The few studies that have been published on this subject specifically focus on the left ventricle or papillary muscle (Bouzeghrane et al. 2005; Vracko et al. 1990). Moreover, the studies are limited to one time point and do not compare both sexes; therefore, they might have overlooked potential age- and/or sex-dependent differences in the spatial arrangement of fibrillin-1 in the myocardial tissue.

Knowledge of the spatial arrangement of fibrillin-1 throughout the entire normal murine myocardial tissue is essential for future experimental set-ups of studies evaluating the impact of pathological changes associated with fibrillin-1 pathogenic variants on the myocardial tissue. Pathogenic variants in *FBN1* cause Marfan syndrome, an autosomal dominantly inherited connective tissue disorder with clinical manifestations mainly in the ocular, skeletal and cardiovascular system (Campens et al. 2015; De Backer et al. 2006; De Backer 2009). Patients with Marfan syndrome are prone to develop intrinsic cardiomyopathy, however, the exact underlying disease mechanism is yet to be unravelled (Alpendurada et al. 2010; Campens et al. 2015; Cook et al. 2014; Hetzer et al. 2016; De Backer 2009). Our group associated a reduced fibrillin-1 deposition in the myocardial tissue with a deterioration of the left ventricular function in 6 months old mice harbouring a missense mutation (C1039G/+) in the *Fbn1* gene (Campens et al. 2015). This implies that the microfibrillar network serves an important role in the mechanical properties of the myocardium. Moreover, based on the study of Cook et al. performed in hypomorphic *Fbn1* mutant mgR/mgR mice presenting a severe form of Marfan syndrome, fibrillin-1 is a force-transmitting molecule crucial for the mechanosignaling in the mammalian heart (Cook et al. 2014).

In this study, we evaluated the spatial arrangement of fibrillins throughout the entire wild-type murine myocardial tissue by means of (immuno)histochemistry. Male and female mice were studied at the ages of 1, 3 and 6 months, based on the time span of our previous study (Campens et al. 2015). In addition, collagen and elastin staining was performed as reference.

Materials and methods

Mice

Male and female wild-type C57BL/6J mice, aged 1, 3 and 6 months, were used for this study ($n=3$ mice/time point/sex). All applicable international, national and/or institutional guidelines for the care and use of animals were followed. All procedures performed in this study involving animals were in accordance with the ethical standards of the Ethics Committee of the Ghent University Hospital (permit number: ECD17/07).

Immunofluorescence and histological staining

Mice were sacrificed by means of CO_2-inhalation (1.0 L/min). Subsequently, a thoracotomy was performed and the heart was flushed with 1x phosphate buffered saline (PBS) and dissected. Next, the hearts were fixed for 20 h in 4% paraformaldehyde (PFA). Following fixation, the hearts were dehydrated and embedded in paraffin per routine histological procedure (Leica TP1020 tissue processor, Leica biosystems). Five µm thick sections were cut at the level of the apex, mid-ventricles and atria as presented in Online Resource 1 (Microm HM355S, Thermo Scientific). Additionally, 5-µm thick transverse sections of the heart of an

extra 6 months old female mouse were acquired in which apical, ventricular and atrial myocardial tissue was present within the same tissue section (Online Resource 1). Before staining, the sections were deparaffinised and rehydrated by passage through 100% xylene, graded ethanol (100, 90, and 70%) and distilled water.

For immunofluorescence staining, epitopes of interest were unmasked by means of heat-induced antigen-retrieval with 10 mM sodium citrate pH 6 using a pressure cooker (2100 Retriever, Laborimpex - BaseClear Lab Products) (Fowler et al. 2011). Subsequently, the sections were washed twice in distilled water and once in tris-buffered saline with 0.05% Tween 20 (TBST). Next, nonspecific binding was blocked by incubation with 5% bovine serum albumin (BSA, Sigma-Aldrich) for 1 h at room temperature (RT). Fibrillin-1 and -2 were detected by overnight incubation at 4 °C in a humidified chamber with a polyclonal antibody directed against fibrillin-1 (rabbit pAb 9543) and fibrillin-2 (mouse pAb 0868) diluted 1/100 in TBST containing 5% BSA. Afterwards, sections were incubated for one hour at RT in a dark humidified chamber either with DyLight™ 633 goat anti-rabbit IgG (H + L) (1/1000; Fisher Scientific) or Alexa Fluor® 488 goat anti-mouse IgG (H + L) (1/100; Life Technologies Europe). Finally, anti-fade mounting medium with DAPI (H-1200, Vectashield) was added and sections were coverslipped. Nonspecific staining was verified by omission of the primary antibody.

In addition to a standard Hematoxylin & Eosin staining (Cardiff et al. 2014), a Picrosirius Red (collagen) (Junqueira et al. 1979) and Verhoeff-Van Gieson (elastin) (Kazlouskaya et al. 2013) staining was performed according to standard protocols.

Sections were visualised using a Zeiss Axio fluorescence microscope (Observer.Z1, Carl Zeiss microimaging) coupled to an Axiocam 506 mono camera (6 mega pixels, Zeiss) with analog gain of 2×. All tissue sections were exposed for 800 ms to the excitation wavelength and images were obtained at a magnification of 10× or 40× with objectives EC "Plan-Neofluar" 10×/0.30 and LD "Plan-Neofluar" 40×/0.6, respectively (both from Zeiss). Images of 1376 × 1104 px (pixel size 9.08 × 9.08 µm) were taken at an image bit depth of 16 after which the threshold of every image was equalized based on the threshold of an image with a very intense fluorescent signal. To obtain an overview-image of the entire section, stitching software (Tiles-Zeiss, ZEN pro 2012 (blue edition), Carl Zeiss microimaging) was used. The mean fluorescence intensity of the fibrillin-1 staining was measured to give an impression of the amount of fibrillin-1 present (Image analysis software, ZEN pro 2012 (blue edition), Carl Zeiss microimaging). For intensity measurements at the level of the mid-ventricular tissue section the subepicardial, outer compact myocardial and inner trabeculated myocardial area was manually selected based on histology (Scudamore 2014). Any histological artefacts within the tissue sections were excluded from these measurements. Figures were made with Adobe Illustrator CC 2017 (Adobe Creative Cloud 2017.1.0-version).

Western blotting

Hearts dissected from 3 additional 3-months-old female wild-type mice were subdivided into apical, mid-ventricular and atrial myocardial tissue samples. Subsequently, tissue samples were homogenized by mixing in lysis buffer (RIPA, Sigma-Aldrich) complemented with protease inhibitors (Complete protease inhibitor cocktail tablets, Roche) and phosphatase inhibitors (Cocktail II and III, Sigma-Aldrich) at a 30% (v/w) ratio. Lysates were centrifuged at 14,000 rpm at 4 °C for 30 min and supernatants were collected and stored at − 80 °C until further processing. Protein concentration was determined using the Pierce BCA (bicinchoninic acid) 562 nm Protein assay kit (Thermo Fisher Scientific). Protein samples (50 µg) diluted to a total volume of 20 µl with PBS were reduced by adding 2 µl 1M dithriothreitol (Sigma-Aldrich) and incubation at 95 °C for 5 min. Next, samples were loaded on a NuPage 3–8% Tris–Acetate gel (Invitrogen) together with 5× non-reducing lane marker sample buffer (Thermo Fisher Scientific). Following SDS-PAGE electrophoresis, proteins were transferred onto a PVDF membrane (Invitrogen) by means of the iBlot 2 dry blotting system (Thermo Fisher Scientific). The membrane was blocked in 3% BSA buffer (Sigma-Aldrich) for one hour and incubated overnight at 4 °C with primary antibodies. Primary antibodies used are: rabbit polyclonal antibody directed against fibrillin-1 (1:1000, pAb 9543) and rabbit polyclonal antibody directed against vinculin (1:1000, Cell Signaling Technology) was used as loading control. Next, membranes were incubated with a secondary antibody, anti-rabbit IgG HRP-linked (1:5000, Cell Signaling Technologies) for 1 h at RT. Subsequently, membranes were incubated with the SuperSignal West Dura luminol-based ECL HRP substrate (Thermo Fisher Scientific) for 5 min at RT. Membranes were scanned using the Amersham Imager 680 (GE Healthcare Life Sciences). Quantification of the immunoblots was performed using Image J software (v. 1.44p).

Statistical analysis

IBM® SPSS® Statistics version 24 was used for statistical analysis and generating graphs. Student's *t* test or one-way ANOVA, followed by a post hoc Tukey test were used for normally distributed data. Otherwise, Mann–Whitney *U* tests or Kruskal–Wallis tests were performed. All values were normalized to the highest value. A p value of < 0.05 was used to define statistical significance (two-sided).

Policy on antibody validation

pAbs 9543 and 0868 have been previously described and demonstrated to bind specifically to epitopes present in fibrillin-1 and fibrillin-2, respectively (Charbonneau et al. 2003, 2010; Kuo et al. 2007; Reinhardt et al. 1996; Sakai et al. 1986).

Results

Immunofluorescence staining intensity

"Myocardial tissue" sections from the hearts of male and female wild-type C57BL/6J mice, aged 1, 3 and 6 months, were stained for fibrillin-1 and -2. Fluorescent staining of fibrillin-1 was observed in cross-sections of the atria, mid-ventricles and apex (Online Resource 1) of both male and female mice and at each of the studied time-points.

No significant difference in the intensity of the fluorescent signal was observed when comparing the cross-sections of different ages and sexes ($p = 0.562$ and $p = 0.856$, respectively) (Fig. 1). However, variation in fibrillin-1 staining was observed in different regions of the heart, with a higher fluorescent signal in the atria compared to the apex and mid-ventricles ($p < 0.001$) (Fig. 2). Western blotting analyses support these results, though large variation in fibrillin-1 content were observed in the myocardial tissue of the apex (Online Resource 2). At the level of the mid-ventricles, fibrillin-1 was mainly present in the subepicardium and the inner trabecular myocardium, whereas the outer compact myocardium showed significantly less fibrillin-1 staining ($p < 0.001$) (Fig. 3). This subdivision based on the staining intensity between the inner trabecular and outer compact myocardium was only observed in the left ventricular wall. As for the free right ventricular wall, staining intensities did not differ across the wall. In addition, the intensity of the fibrillin-1 staining in the right free ventricular wall was similar to that in the subepicardium of the left ventricular wall. No significant difference was observed between the right and left atrium ($p = 0.083$) (Fig. 3). In contrast to fibrillin-1, fibrillin-2 staining was very limited in all the cross-sections (Online Resource 3).

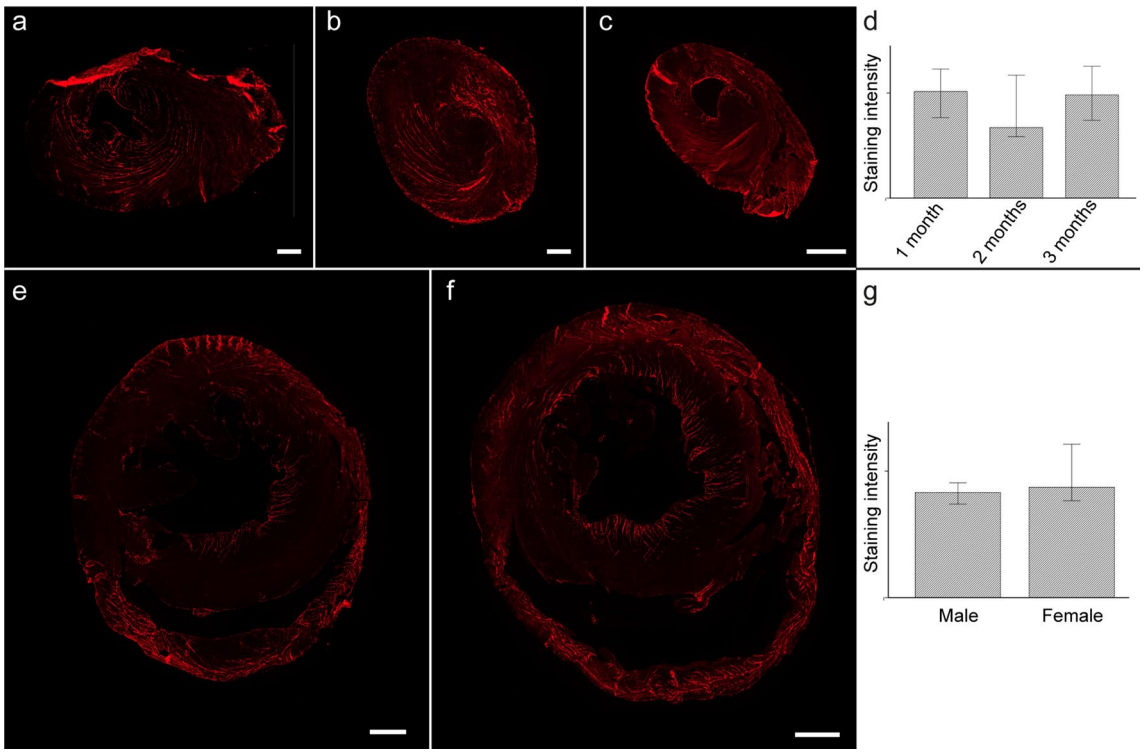

Fig. 1 Fibrillin-1 expression in myocardial tissue of male and female mice at 1, 3 and 6 months of age. Myocardial tissue cross-sections were stained with pAb 9543 directed against fibrillin-1 (red). **a**–**c** Apical cross-sections of female mice at the age of 1, 3 and 6 months, respectively. **d** No significant difference in staining intensity could be observed between the different age groups ($p = 0.562$, $n = 6$ mice per group). **e, f** Cross-sections at the level of the mid-ventricles of a female and male mouse (aged 1 month). **g** Sex does not influence fibrillin-1 expression ($p = 0.856$, $n = 9$ mice per group). Selected images are representative for the studied subgroups. Bars indicate the median staining intensity normalized to the highest value and error bars indicate 95% confidence interval. Scale bars of images **a, b** 200 µm, scale bars of images **c**–**f** 500 µm

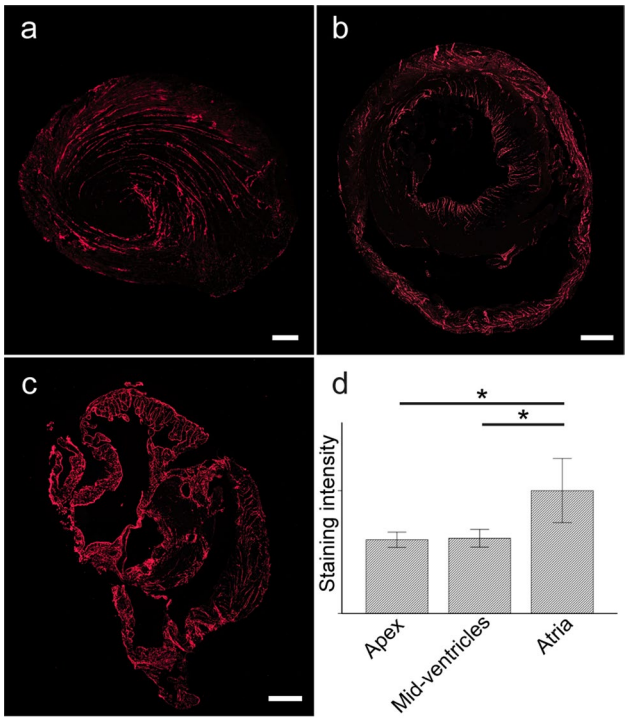

Fig. 2 Fibrillin-1 distribution in different myocardial regions. **a–c** Cross-sections of the heart of a female wild-type mouse (age 1 month) at the level of the apex, mid-ventricles and atria, respectively. **d** Fibrillin-1 staining intensity (red) was significantly higher at the level of the atria compared to the mid-ventricles and apex ($p < 0.001$, $n = 18$ mice). Similar results were obtained in all sections, independent of sex or age. Bar chart indicates the mean staining intensity and error bars indicate standard deviations. Scale bar of image **a** 200 µm, scale bars of images **b, c** 500 µm. *p value < 0.001

Spatial arrangement of fibrillin

Myocardial tissue

Fibrillin-1 presented as long fibres at the level of the perimysium of the apical region, running parallel to the cardiac muscle fibres (Fig. 4a, b). Although the muscle fibres were oriented differently, a similar staining pattern could be observed at the level of the trabecular myocardium of the mid-ventricular region (Fig. 4c, d). A limited amount of fibrillin-1 strands was observed at the level of the compact myocardium of the mid-ventricular region. These strands seemed to emerge as extensions from the fibrillin-1 present in the inner trabecular myocardium (Fig. 4e, arrow). In the subepicardium, microfibrils formed a loose network-like pattern rather than parallel fibres (Fig. 4f).

The thick endocardium lining the lumen of the atria was rich in fibrillin-1 fibres (Fig. 4g, h). In addition, fibrillin-1 was also occasionally located at the level of the endomysium (Fig. 4h, arrowheads).

In addition to immunofluorescence staining for fibrillin-1 and -2, we performed standard histological staining for collagen and elastic fibres (Fig. 5). Fibrillin-1 and collagen showed a similar distribution pattern. Little elastic fibre staining was observed in the peri- and endomysium of the apex and mid-ventricles. In contrast, elastic fibres were abundantly present in the endocardium of the atria as expected based on the literature (Lowe and Anderson 2015) (Fig. 5e).

Valves

Fibrillin-1 staining in the aortic valve leaflet was mainly restricted to the lamina fibrosa and lamina radialis (Fig. 5g). In contrast, collagen staining was seen throughout the entire aortic valve leaflet whereas elastic fibres were rather scarce (Fig. 5i). No difference in the spatial arrangement of fibrillin-1, collagen and elastic fibres was observed in the pulmonary, mitral and tricuspid valve compared to the aortic valve (results not shown).

Coronary arteries

Around the vessels of the coronary system abundant fibrillin-1 and collagen staining was observed. In the vessel wall itself, fibrillin-1 and elastin staining was present in the tunica media and collagen is located in the tunica adventitia of the vessel (Fig. 5).

Discussion

This study aimed to contribute to a better understanding of the spatial arrangement of fibrillins in normal murine myocardial tissue. We confirmed that fibrillin fibres are major constituents of the myocardial ECM and furthermore observed that their spatial arrangement within the myocardial tissue is independent of age and sex but highly region-dependent.

No difference in fibrillin-1 staining intensity could be observed between male and female mice. This implies that normal levels of sex hormones do not influence fibrillin-1 deposition in wild-type murine myocardial tissue. Previously, however, it has been published that oestrogen administration can have an effect on the ECM-composition of the myocardial tissue in prevention of adverse myocardial remodelling (Voloshenyuk and Gardner 2010). Both observations should be taken into account when investigating the impact of fibrillin-1 dysfunction on the myocardial tissue.

When comparing the fibrillin-1 staining intensity between the different age groups no significant changes could be observed either. The observation that age does not influence fibrillin-1 deposition was also reported by Hanssen et al.

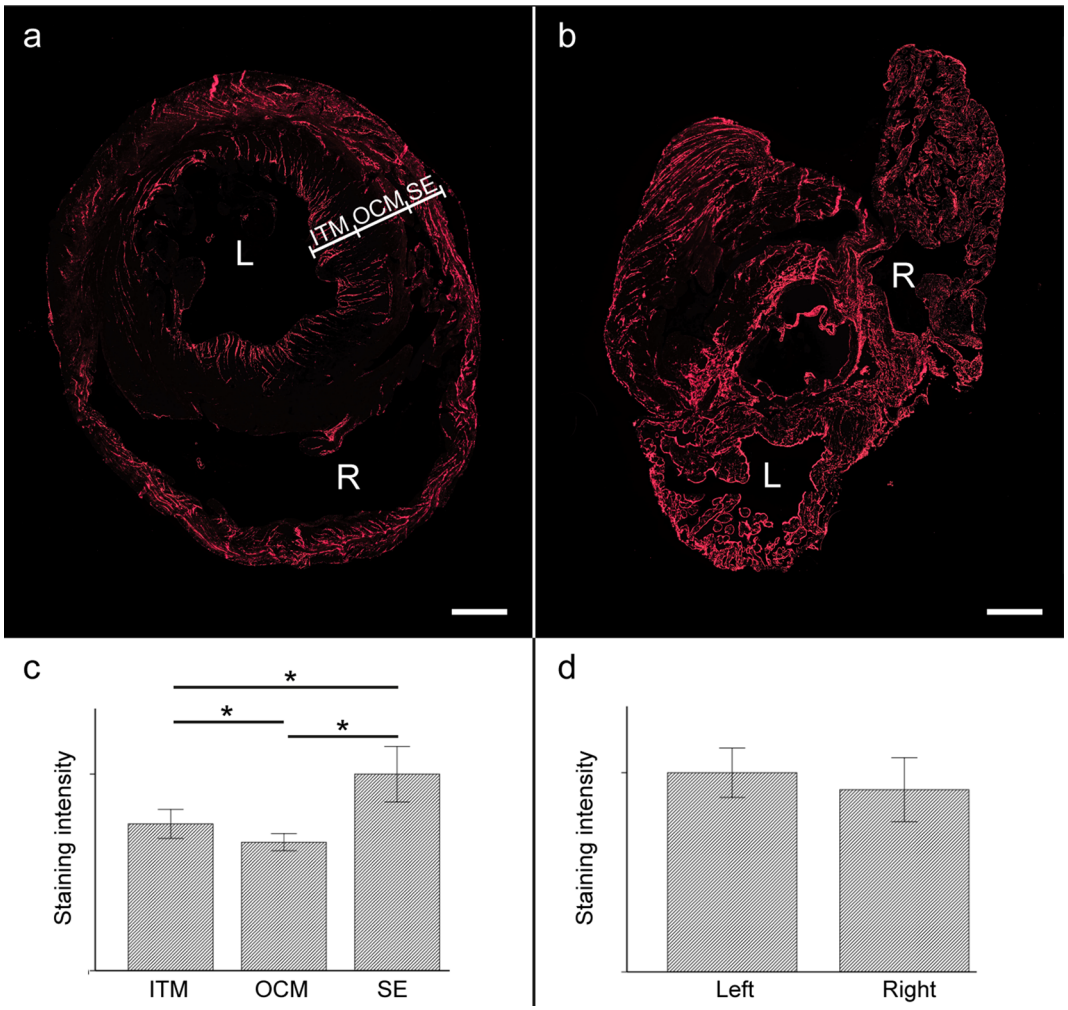

Fig. 3 Fibrillin-1 distribution at the level of the mid-ventricles and the atria. **a** Cross-section at the level of the mid-ventricles of the heart of a female mouse of 1 month old. **c** Fibrillin-1 staining intensity (red) differs significantly between the ventricular myocardial layers with highest staining intensity in the subepicardium and inner trabecular myocardium compared to the outer compact myocardium ($p < 0.001$, $n = 18$ mice). **b** Myocardial tissue cross-section at the level of the atria. **d** No significant difference in fibrillin-1 staining intensity could be observed between the left and right atrium ($p = 0.083$). Graphs include data from all subgroups (female/male and all ages). Histograms show means and standard deviation. Scale bars = 500 µm. *SE* subepicardium, *OCM* outer compact myocardium, *ITM* inner trabecular myocardium, *R* right, *L* left. **p* value < 0.001

(Hanssen et al. 2001). They studied fibrillin-1 expression in the ocular system of a guinea pig model. In this model, the fibrillin-1 mRNA expression in the microfibril-rich zonular fibres decreased from birth to old age whereas a constant level of fibrillin-1 protein expression was observed. Based on this observation, the authors suggested a slow turn-over of fibrillin-1 in the zonular fibres of the eye (Hanssen et al. 2001). Possibly, this could also be true for cardiac fibrillin-1.

Based on both the immunofluorescence staining and western blotting analyses, the presence of fibrillin-1 appears to be region-dependent with significantly more fibrillin-1 staining in the atria compared to the mid-ventricles and apex. This observation could be due to the fact that the atria contain more ECM compared to the ventricles and as a result more fibrillin-1 might be deposited (Burstein et al. 2008). Another possible explanation for this finding might be the difference in thickness of the endocardium between the atria and the ventricles. More specifically, the fibroelastic layer of the endocardium, composed of substantial amounts of elastin fibres and, therefore, microfibrils, is thicker in the atria compared to the ventricles (Lowe and Anderson 2015). Hence, more fibrillin-1 deposition can be expected in the atrial endocardium compared to the ventricular endocardium, explaining the higher fluorescent signal. This fibrillin-rich fibroelastic layer, in combination with the trabeculated structure of the atrium, allows extensive stretching of the atrial wall, which facilitates the blood flow between the

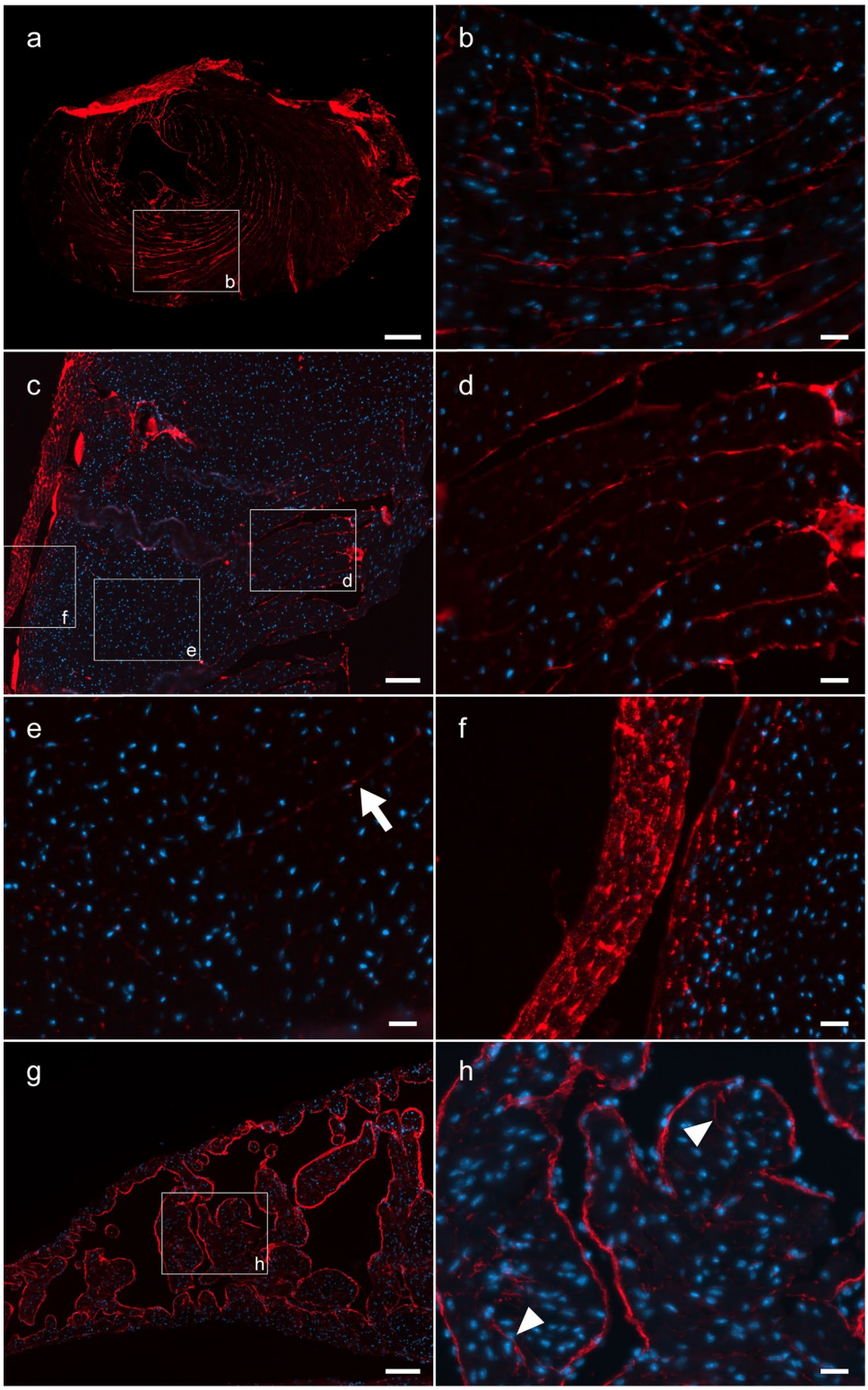

Fig. 4 Fibrillin-1 is present as long fibres throughout the entire myocardial tissue. Cross-sections of female murine myocardial tissue (age 1 month) were stained with pAb 9543 directed against fibrillin-1 (red) and nuclear DAPI (blue). **a, b** Apical cross-section of the myocardial tissue show long fibres of fibrillin-1 at the level of the perimysium. **c** Myocardial tissue section at the level of the left ventricular free wall with higher magnification pictures at the level of the inner trabecular myocardium (**d**), outer compact myocardium (**e**) and subepicardium (**f**). The trabecular and compact myocardium are characterized by fibrillin-1 microfibrils organized in a parallel fashion, whereas the subepicardium shows a loose-network of fibrillin-1 fibrils. The arrow in figure **e** indicates fibrillin-1 strand penetrating the compact myocardium. **g, h** Myocardial tissue section at the level of the left atrium. Fibrillin-1 is mainly present at the level of the endocardium. Arrowheads in image **h** indicate endomysial fibrillin-1. Scale bar image **a** 200 µm, scale bars images **b–f, h** 20 µm, scale bars images **c, g** 100 µm

atrium and ventricle at relatively low venous blood pressures (Brandenburg et al. 2016). Furthermore, the variation of fibrillin-1 expression observed in apical myocardial tissue by western blotting might be due to the significantly smaller amount of tissue sampled from the apex compared to the mid-ventricular and atrial myocardial samples inherent to the anatomy of the heart. Differences in specific tissue composition of these apical samples might explain the fibrillin-1 expression heterogeneity that was observed [e.g., a major blood vessel might be present in the apical

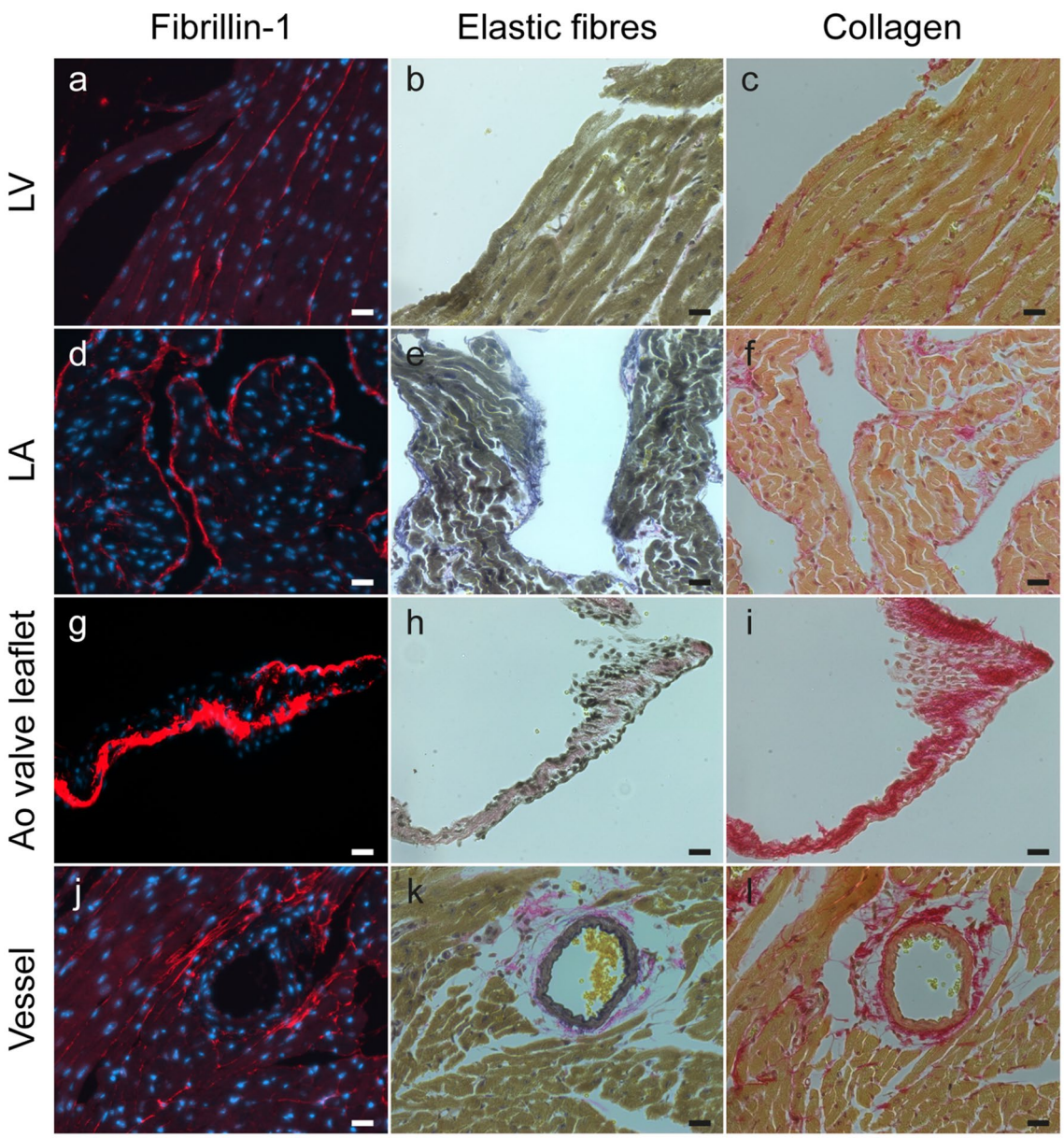

Fig. 5 Localisation of myocardial ECM components in the murine myocardial tissue. Serial sections were stained for fibrillin-1 and nuclear DAPI [red and blue, respectively (**a, d, g, j**)], elastic fibres (black, images **b, e, h, k**) and collagen (red-magenta, images **c, f, i, l**). Detailed pictures of the left ventricular wall, left atrium, aortic valve leaflet and a small vessel embedded in the myocardial tissue are shown. Collagen shows a similar staining distribution as fibrillin-1 in the left ventricular wall, the left atrium and the connective tissue surrounding the small vessels embedded in the myocardial tissue. The main component of the aortic valve leaflet is collagen, whereas fibrillin-1 is mainly observed at the level of the lamina fibrosa and the lamina radialis of the leaflets. Elastic fibres are abundantly present in the endocardium of the atrium, the tunica media of the aorta wall and small vessels. Scale bars = 20 µm. *LV* left ventricle, *LA* left atrium, *Ao* aorta

myocardial tissue sample loaded in the third lane of the western blot setup (Online resource 2)].

At the level of the mid-ventricles we observed a clear difference in fibrillin-1 distribution between the inner trabecular myocardium, the outer compact myocardium and the subepicardium of the left ventricle. Throughout the cardiac cycle the left ventricle undergoes large changes in shape and dimension (Pope et al. 2008). The extent of these structural changes is greater at the level of the inner trabecular myocardium compared to the outer compact myocardium (Pope et al. 2008). We demonstrated a higher fibrillin-1 deposition at the level of the inner trabecular myocardium compared to the outer compact myocardium. This spatial arrangement of fibrillin-1 combined with its

elastic properties suggests an important role of fibrillin fibres in enabling and supporting the structural changes of the left ventricle without the risk of overextension of the cardiac myocytes (Bouzeghrane et al. 2005; Pope et al. 2008). Moreover, since few elastic fibres seem to be present in the ECM of the ventricular myocardium, fibrillin fibres are mainly accountable for providing elasticity to the ventricular myocardial tissue (Mizuno et al. 2005). The high deposition of fibrillin-1 in the subepicardium is due to its accommodation of multiple coronary vessels and their dense surrounding fibrillin-rich connective tissue. In addition, the irregular organisation of multiple vessels in the subepicardium results in a loose network-like distribution pattern of fibrillin-1 (Pope et al. 2008). This particular spatial arrangement of fibrillin-1 within the left ventricular wall is not observed in the right ventricular wall, mainly because the myocardium of the right ventricle is not as strongly developed as the left ventricular myocardium due to the lower pressure in the pulmonary circulation.

In the cardiac valves, fibrillin-1 is mainly located in the lamina fibrosa and lamina radialis (Votteler et al. 2013). These layers are known to facilitate the movement of the leaflets which could be accountable to the elastic properties of fibrillin-1 (Hinton and Yutzey 2011). Although fibrillin-1 has been reported to be present in the lamina spongiosa, we were unable to detect them in the present study as fibrillin-1 epitopes were probably masked (Votteler et al. 2013). Collagen was observed in many of the regions where fibrillin-1 staining was shown. This implies a potential interplay between the stiffness of collagen and the elasticity of the fibrillin fibres in providing the right mechanical properties to the environment to ensure a proper functioning heart.

In contrast to fibrillin-1, very limited amounts of fibrillin-2 staining could be observed in the cardiac tissue. This does not necessarily mean that fibrillin-2 is not present in wild-type murine myocardial tissue. Charbonneau et al. showed that postnatal deposition of fibrillin-1 molecules occurs around a core of fibrillin-2 expressed and assembled during foetal development, subsequently masking fibrillin-2 epitopes (Charbonneau et al. 2010).

In conclusion, our observations confirm the notion that fibrillin fibres are major connective tissue components of the myocardial ECM and their specific spatial arrangement suggest a role in enabling and supporting the structural changes of the myocardial tissue. Importantly, this is the first study to image the presence of the fibrillins in the entire myocardial tissue (from base to apex) of mice of different age and sex. Insights into the spatial arrangement of fibrillin in physiological conditions are crucial for future experimental set-ups of studies evaluating pathophysiological conditions, such as Marfan syndrome.

Limitations

(Immuno)histochemistry can be used to obtain a rough idea of the amount of protein present in tissues, however, it is important to realize that it is a semi-quantitative technique. Furthermore, differences in immunofluorescence signal intensity might reflect accessibility of the epitopes as a consequence of structural arrangement of the fibrillin fibres rather than a difference in the amount of protein present. However, since we carefully performed heat mediated antigen-retrieval we assume that the fibrillin-1 proteins present in the tissue sections have been irreversibly unfolded and, therefore, epitopes are accessible for antibody staining (Fowler et al. 2011). Additionally, confirmation with a second antibody directed against fibrillin-1 or fibrillin-2 has not been performed. However, pAb 9543 and pAb 0868 have already been proven to bind very specifically to fibrillin-1 and fibrillin-2, respectively (Charbonneau et al. 2003, 2010; Kuo et al. 2007; Reinhardt et al. 1996; Sakai et al. 1986).

Acknowledgements We are grateful to Dr. Lynn Sakai for providing the fibrillin antibodies pAb 9543 and pAb 0868. Julie De Backer is supported as Senior Clinical Investigator by the Research Foundation Flanders and Marjolijn Renard is supported as Post Doc Researcher by the Research Foundation Flanders.

Compliance with ethical standards

Conflict of interest The authors declare that they have no conflict of interest.

References

Alpendurada F, Wong J, Kiotsekoglou A, Banya W, Child A, Prasad SK, Pennell DJ, Mohiaddin RH (2010) Evidence for Marfan cardiomyopathy. Eur J Heart Fail 12(10):1085–1091. https://doi.org/10.1093/eurjhf/hfq127

Borg TK, Rubin K, Carver W, Samarel A, Terracio L (1996) The cell biology of the cardiac interstitium. Trends in Cardiovasc Med 6(2):65–70. https://doi.org/10.1016/1050-1738(96)00005-9

Bouzeghrane F, Reinhardt DP, Reudelhuber TL, Thibault G (2005) Enhanced expression of fibrillin-1, a constituent of the myocardial extracellular matrix in fibrosis. Am J Physiol Heart Circ Physiol 289(3):H982-H991. https://doi.org/10.1152/ajpheart.00151.2005

Brandenburg S, Arakel EC, Schwappach B, Lehnart SE (2016) The molecular and functional identities of atrial cardiomyocytes in health and disease. Biochim Biophys Acta; Mol Cell Res 1863(7):1882–1893. https://doi.org/10.1016/j.bbamcr.2015.11.025

Burstein B, Libby E, Calderone A, Nattel S (2008) Differential behaviors of atrial versus ventricular fibroblasts - A potential role for platelet-derived growth factor in atrial-ventricular remodeling differences. Circ 117(13):1630–1641. https://doi.org/10.1161/circulationaha.107.748053

Cain SA, Morgan A, Sherratt MJ, Ball SG, Shuttleworth CA, Kielty CM (2006) Proteomic analysis of fibrillin-rich microfibrils. Proteomics 6(1):111–122. https://doi.org/10.1002/pmic.200401340

Campens L, Renard M, Trachet B, Segers P, Mosquera LM, De Sutter J, Sakai L, De Paepe A, De Backer J (2015) Intrinsic cardiomyopathy in Marfan syndrome: results from in-vivo and ex-vivo studies of the Fbn1(C1039G/+) model and longitudinal findings in humans. Pediatr Res 78(3):256–263. https://doi.org/10.1038/pr.2015.110

Cardiff RD, Miller CH, Munn RJ (2014) Manual hematoxylin and eosin staining of mouse tissue sections., vol 6. Cold Spring Harbor Laboratory Press.

Charbonneau NL, Dzamba BJ, Ono RN, Keene DR, Corson GM, Reinhardt DP, Sakai LY (2003) Fibrillins can co-assemble in fibrils, but fibrillin fibril composition displays cell-specific differences. J Biol Chem 278(4):2740–2749. https://doi.org/10.1074/jbc.M209201200

Charbonneau NL, Jordan CD, Keene DR, Lee-Arteaga S, Dietz HC, Rifkin DB, Ramirez F, Sakai LY (2010) Microfibril structure masks fibrillin-2 in postnatal tissues. J Biol Chem 285(26):20242–20251. https://doi.org/10.1074/jbc.M109.087031

Cook JR, Carta L, Benard L, Chemaly ER, Chiu E, Rao SK, Hampton TG, Yurchenco P, Costa KD, Hajjar RJ, Ramirez F, Gen TACRC. (2014) Abnormal muscle mechanosignaling triggers cardiomyopathy in mice with Marfan syndrome. J Clin Invest 124(3):1329–1339. https://doi.org/10.1172/jci71059

Corson GM, Charbonneau NL, Keene DR, Sakai LY (2004) Differential expression of fibrillin-3 adds to microfibril variety in human and avian, but not rodent, connective tissues. Genomics 83(3):461–472. https://doi.org/10.1016/j.ygeno.2003.08.023

De Backer J (2009) The expanding cardiovascular phenotype of Marfan syndrome. Eur J Echocardiogr 10(2):213–215. https://doi.org/10.1093/ejechocard/jen311

De Backer JF, Devos D, Segers P, Matthys D, Francois K, Gillebert TC, De Paepe AM, De Sutter J (2006) Primary impairment of left ventricular function in Marfan syndrome. Int J Cardiol 112(3):353–358. https://doi.org/10.1016/j.ijcard.2005.10.010

Fowler CB, Evers DL, O'Leary TJ, Mason JT (2011) Antigen retrieval causes protein unfolding: evidence for a linear epitope model of recovered immunoreactivity. J Histochem Cytochem 59(4):366–381. https://doi.org/10.1369/0022155411400866

Hanssen E, Franc S, Garrone R (2001) Synthesis and structural organization of zonular fibers during development and aging. Matrix Biol 20(2):77–85. https://doi.org/10.1016/s0945-053x(01)00122-6

Hetzer R, Siegel G, Walter EMD (2016) Cardiomyopathy in Marfan syndrome. Eur J CardioThorac Surg 49(2):561–568. https://doi.org/10.1093/ejcts/ezv073

Hinton RB, Yutzey KE (2011) Heart valve structure and function in development and disease. In: Julius D, Clapham DE (eds) Annual Rev Physiol, vol 73, pp 29–46. https://doi.org/10.1146/annurev-physiol-012110-142145

Hubmacher D, El-Hallous EI, Nelea V, Kaartinen MT, Lee ER, Reinhardt DP (2008) Biogenesis of extracellular microfibrils: multimerization of the fibrillin-1 C terminus into bead-like structures enables self-assembly. PNAS 105(18):6548–6553. https://doi.org/10.1073/pnas.0706335105

Jensen SA, Handford PA (2016) New insights into the structure, assembly and biological roles of 10–12 nm connective tissue microfibrils from fibrillin-1 studies. Biochem J 473:827–838. https://doi.org/10.1042/bj20151108

Junqueira LCU, Bignolas G, Brentani RR (1979) Picrosirius staining plus polarization microscopy, a specific method for collagen detection in tissue-sections. Histochem J 11(4):447–455. https://doi.org/10.1007/bf01002772

Kazlouskaya V, Malhotra S, Lambe J, Idriss MH, Elston D, Andres C (2013) The utility of elastic Verhoeff-Van Gieson staining in dermatopathology. J Cutan Pathol 40(2):211–225. https://doi.org/10.1111/cup.12036

Kuo CL, Isogai Z, Keene DR, Hazeki N, Ono RN, Sengle G, Bachinger HP, Sakai LY (2007) Effects of fibrillin-1 degradation on microfibril ultrastructure. J Biol Chem 282(6):4007–4020. https://doi.org/10.1074/jbc.M606370200

Lockhart M, Wirrig E, Phelps A, Wessels A (2011) Extracellular matrix and heart development. Birth Defects Res A Clin Mol Teratol 91(6):535–550. https://doi.org/10.1002/bdra.20810

Lowe JS, Anderson PG (2015) Stevens & lowe's human histology—fourth edition. 4 edn. Elsevier Mosby

Mizuno T, Mickle DAG, Kiani CG, Li RK (2005) Overexpression of elastin fragments in infarcted myocardium attenuates scar expansion and heart dysfunction. Am J Physiol-Heart Circ Physiol 288(6):H2819-H2827. https://doi.org/10.1152/ajpheart.00862.2004

Pope AJ, Sands GB, Smaill BH, LeGrice IJ (2008) Three-dimensional transmural organization of perimysial collagen in the heart. Am J Physiol Heart Circ Physiol 295(3):H1243-H1252. https://doi.org/10.1152/ajpheart.00484.2008

Purslow P (2008) The extracellular matrix of skeletal and cardiac muscle. In: Collagen: structure & mechanics. Springer, Boston, pp 325–357

Ramirez F, Pereira L (1999) The fibrillins. Int J Biochem Cell Biol 31(2):255–259. https://doi.org/10.1016/s1357-2725(98)00109-5

Reinhardt DP, Keene DR, Corson GM, Poschl E, Bachinger HP, Gambee JE, Sakai LY (1996) Fibrillin-1: Organization in microfibrils and structural properties. J Mol Biol 258(1):104–116. https://doi.org/10.1006/jmbi.1996.0237

Sakai LY, Keene DR, Engvall E (1986) Fibrillin, a new 350-KDa glycoprotein, is a component of extracellular microfibrils. J Cell Biol 103(6):2499–2509. https://doi.org/10.1083/jcb.103.6.2499

Sakai LY, Keene DR, Renard M, De Backer J (2016) FBN1: The disease-causing gene for Marfan syndrome and other genetic disorders. Gene 591(1):279–291. https://doi.org/10.1016/j.gene.2016.07.033

Scudamore CL (2014) A practical guide to the histology of the mouse. Wiley

Sherratt MJ, Wess TJ, Baldock C, Ashworth JL, Purslow PP, Shuttleworth CA, Kielty CM (2001) Fibrillin-rich microfibrils of the extracellular matrix: ultrastructure and assembly. Micron 32(2):185–200. https://doi.org/10.1016/s0968-4328(99)00082-7

Voloshenyuk TG, Gardner JD (2010) Estrogen improves TIMP-MMP balance and collagen distribution in volume-overloaded hearts of ovariectomized females. Am J Physiol 299(2):R683-R693. https://doi.org/10.1152/ajpregu.00162.2010

Votteler M, Berrio DAC, Horke A, Sabatier L, Reinhardt DP, Nsair A, Aikawa E, Schenke-Layland K (2013) Elastogenesis at the onset of human cardiac valve development. Development 140(11):2345–2353. https://doi.org/10.1242/dev.093500

Vracko R, Thorning D, Frederickson RG (1990) Spatial arrangement of microfibrils in myocardial scars—application of antibody ot fibrillin. J Mol Cell Cardiol 22(7):749–757. https://doi.org/10.1016/0022-2828(90)90087-i

Zhang H, Apfelroth SD, Hu W, Davis EC, Sanguineti C, Bonadio J, Mecham RP, Ramirez F (1994) Structure and expression of fibrillin-2, a novel microfibrillar component preferentially located in elastic matrices. J Cell Biol 124(5):855–863. https://doi.org/10.1083/jcb.124.5.855